



# RAB18 Loss Interferes With Lipid Droplet Catabolism and Provokes Autophagy Network Adaptations

Fazilet Bekbulat<sup>1,†</sup>, Daniel Schmitt<sup>1,†</sup>, Anne Feldmann<sup>1</sup>, Heike Huesmann<sup>1</sup>, Stefan Eimer<sup>2</sup>, Thomas Juretschke<sup>3</sup>, Petra Beli<sup>3</sup>, Christian Behl<sup>1</sup> and Andreas Kern<sup>1</sup>

**1 - Institute of Pathobiochemistry**, University Medical Center of the Johannes Gutenberg University Mainz, Duesbergweg 6, 55128 Mainz, Germany

**2 - Department of Structural Cell Biology**, Institute for Cell Biology and Neuroscience, Goethe University Frankfurt, Max-von-Laue-Str. 13, 60438 Frankfurt, Germany

**3 - Institute of Molecular Biology (IMB)**, Ackermannweg 4, 55128 Mainz, Germany

**Correspondence to Andreas Kern and Christian Behl:** Institute of Pathobiochemistry, University Medical Center of the Johannes Gutenberg University Mainz, Duesbergweg 6, Mainz, D-55128, Germany. [cbeh@uni-mainz.de](mailto:cbeh@uni-mainz.de), [akern@uni-mainz.de](mailto:akern@uni-mainz.de)

<https://doi.org/10.1016/j.jmb.2019.12.031>

**Edited by Martens Sascha**

## Abstract

Autophagy is dependent on appropriate lipid supply for autophagosome formation. The regulation of lipid acquisition and the autophagy network response to lipid-limiting conditions are mostly elusive. Here, we show that the knockout of the RAB GTPase RAB18 interferes with lipid droplet catabolism, causing an impaired fatty acid release. The resulting reduced lipid-droplet-derived lipid availability influences autophagy and provokes adaptive modifications of the autophagy network. These adjustments include increased expression and phosphorylation of ATG2B as well as augmented formation of the ATG12-ATG5 conjugate. Moreover, ATG9A shows an enhanced phosphorylation at amino acid residues tyrosine 8 and serine 14, resulting in an increased ATG9A trafficking. Via pharmacological inhibition of Y8 phosphorylation, we demonstrate that this ATG9A modification is important to maintain basal autophagy under RAB18 knockout conditions. However, while the network adaptations are sufficient to maintain basal autophagic activity, they are incapable of ensuring autophagy induction upon starvation, which is characterized by an enhanced lipid demand. Thus, here, we define the molecular role of RAB18 in connecting lipid droplets and autophagy, emphasize the significance of lipid droplets as lipid sources for the degradative pathway, and uncover a remarkable autophagy network plasticity, including phosphorylation-dependent ATG9A activation, to compensate reduced lipid availability in order to rescue basal autophagic activity.

© 2019 The Author(s). Published by Elsevier Ltd. This is an open access article under the CC BY license (<http://creativecommons.org/licenses/by/4.0/>).

## Introduction

Macroautophagy (hereafter referred to as autophagy) is the eukaryotic lysosomal degradation pathway that mediates protein and organelle turnover and maintains cellular homeostasis [1]. Autophagic cargo is transported in vesicles, the so-called autophagosomes, to lysosomes for degradation and recycling of building blocks. The generation of

autophagosomes is highly dynamic and increases within minutes upon autophagy induction. Several conditions, including nutrient deprivation or rapamycin treatment, stimulate autophagy and result in activation of the AMP-activated kinase PRKAA1 and/or inhibition of the kinase MTOR [2]. Subsequently, ULK1 kinase is activated by phosphorylation, which is required for autophagosome generation in canonical autophagy [3].

The synthesis of double-membraned autophagosomes starts with a precursor membrane, the phagophore, which originates from specific omega-shaped domains (omegasomes) in the ER membrane [4–6]. The phagophore elongates by the addition of substantial amounts of lipids until it finally closes to form an autophagosome, fully engulfing the autophagic cargo. This process involves a cascade of proteins, including two ubiquitin-like conjugations systems, that mediate the formation of the ATG12-ATG5/ATG16L1 protein complex as well as the lipidation of Atg8 family members, such as MAP1LC3B (shortly LC3) [7]. The phosphatidylinositol-3-phosphate (PI(3)P)-binding protein WIPI2 is targeted to the omegasome and remains associated with the phagophore, where it recruits ATG16L1,

which forms a complex with the ATG12-ATG5 conjugate [8]. This complex shows E3 ligase-like activity that promotes the final step of Atg8 lipidation [9–12]. Lipid-conjugated Atg8 proteins associate with the growing phagophore and are essential for autophagosome formation [13]. The proteins stay (partially) attached to autophagic vesicles, resulting in their subsequent lysosomal degradation.

Besides protein processing, phagophore elongation is highly dependent on sufficient lipid supply [3]. Several cellular organelles or compartments, including the ER, plasma membrane, mitochondria, the Golgi complex, the ER-Golgi intermediate compartment, recycling endosomes [3,14], as well as lipid droplets (LDs) [15–17], have been suggested as sources that donate lipids via vesicles or membrane

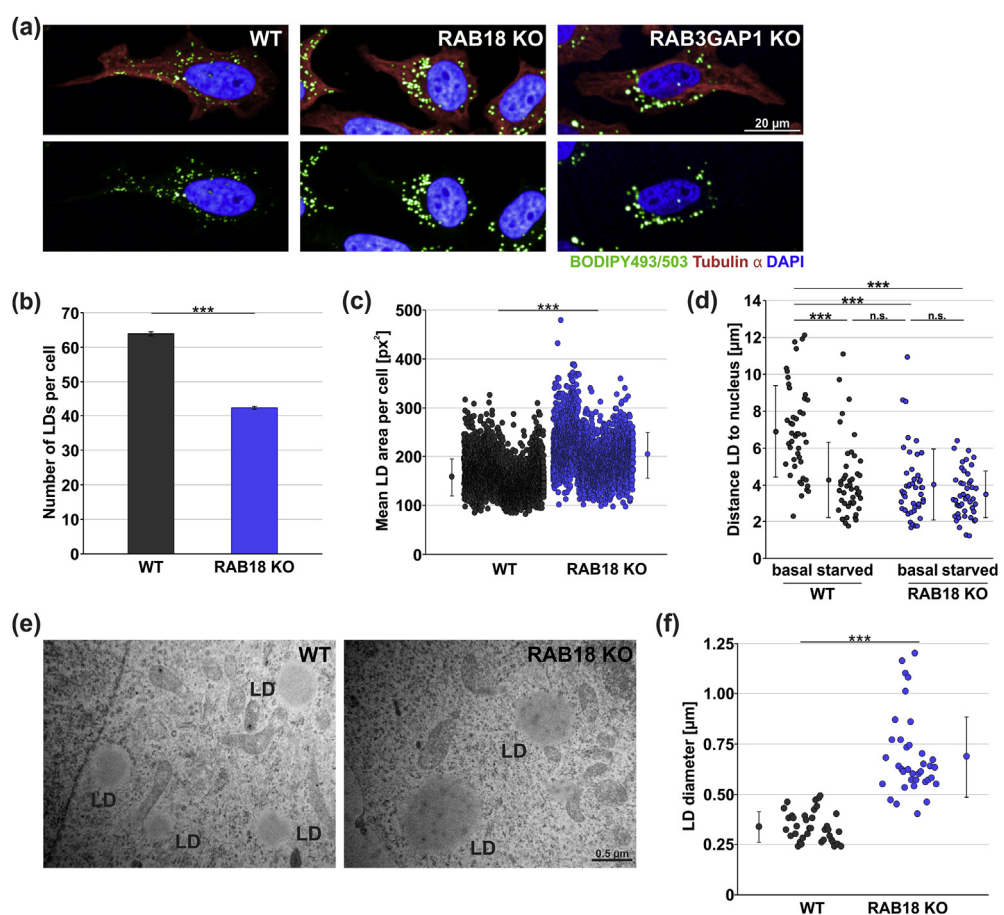


**Fig. 1. The loss of RAB18 function results in an altered LD phenotype. (a)** Representative confocal fluorescence images of LDs stained with BODIPY493/503 (green). Tubulin  $\alpha$  staining (red) served to visualize cell area and DAPI (blue) stained nuclei. Approx. 2500 cells from six independent experiments have been analyzed. **(b)** Statistical analyses of LD number in approx. 2500 single WT and RAB18 KO cells. Statistics are depicted as mean  $\pm$  SEM. n = 6, t-test, \*\*\*P  $\leq$  0.001. **(c)** Analyses of mean LD area in approx. 2500 single WT and RAB18 KO cells. Statistics are depicted as mean  $\pm$  SD. n = 6, t-test, \*\*\*P  $\leq$  0.001. **(d)** Distance of LDs to the nucleus under basal and lipolytic conditions (2 h EBSS) has been analyzed in approx. 45 single WT and RAB18 KO cells from three independent experiments. Statistics are depicted as mean  $\pm$  SD. n = 3, t-test, \*\*\*P  $\leq$  0.001. **(e)** Representative TEM images of LDs in WT and RAB18 KO cells. **(f)** For statistics of LD diameter, approx. 35 individual LDs have been analyzed and statistics are depicted as mean  $\pm$  SD. t-test, \*\*\*P  $\leq$  0.001.

contact sites. However, the detailed process and regulation of autophagic lipid acquisition remain unresolved and the role and importance of LDs as lipid donors for autophagy have been discussed [18].

A key protein involved in autophagic lipid transfer is the multipass transmembrane protein ATG9A that connects the peripheral cellular compartments to autophagosome formation [19–22]. ATG9A directs vesicles from the cellular periphery to the site of phagophore maturation and supplies essential proteins and lipids [23–25]. Under basal autophagy

conditions, the majority of ATG9A is located at the Golgi complex and switches to a dispersed vesicular localization when autophagy is increased. Upon autophagy induction, the specific phosphorylations of ATG9A, mediated by ULK1 and SRC kinase [26,27], are enhanced and foster ATG9A trafficking dynamics, facilitating autophagosome formation.

LDs are lipid sources supporting phagophore elongation that act independently of ATG9A but in close functional association with the ER [15–17]. These cytoplasmic lipid stores are found in virtually all eukaryotic cells and contain neutral lipids, mainly

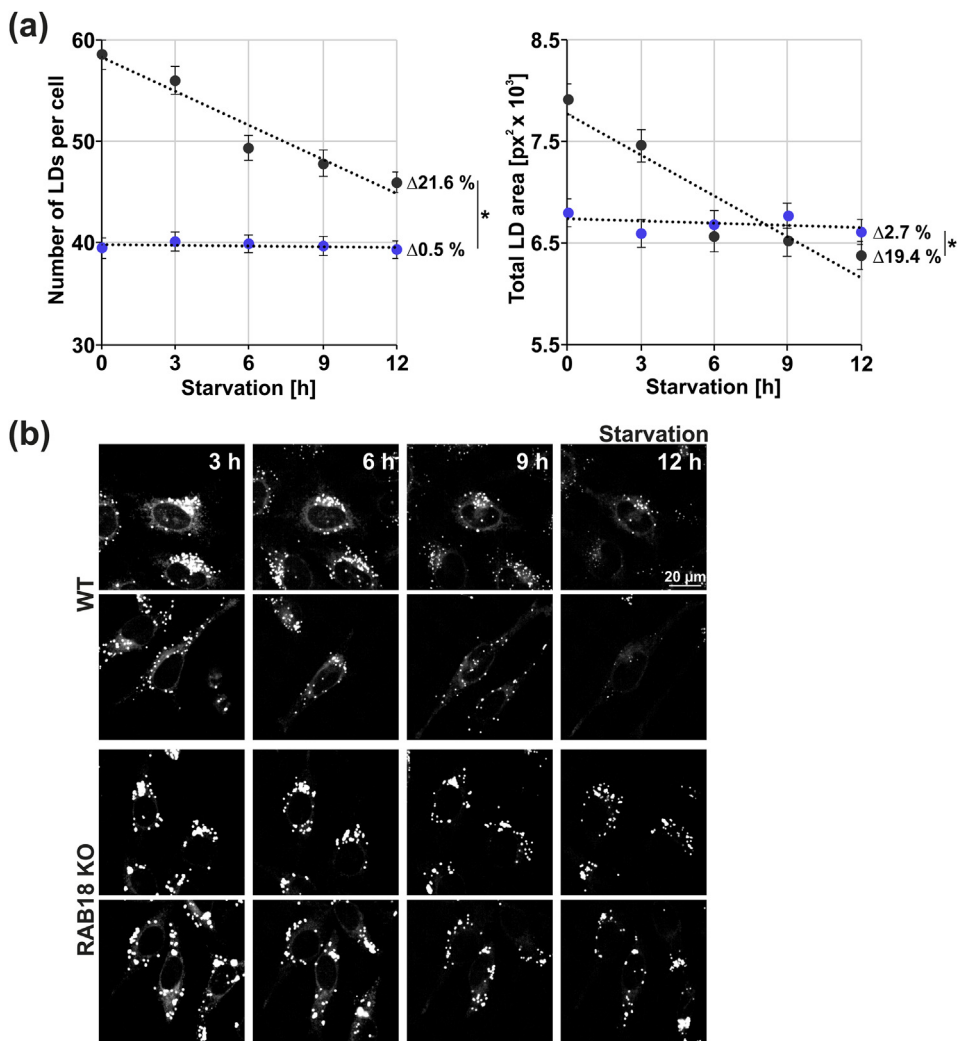


**Fig. 2. The loss of RAB18 impedes fatty acid mobilization from LDs.** (a) LD consumption upon lipolytic conditions (EBSS) in WT (gray) and RAB18 KO cells (blue). LDs were stained with BODIPY493/503. At each indicated time point, the number and total area of LDs in approx. 240 single WT or KO cells from three independent experiments were evaluated. By linear regression comparison, significant differences between the regression coefficients of each condition were analyzed:  $R^2$  LD number: WT = 0.936, KO = 0.162, \*\*\*P  $\leq$  0.001;  $R^2$  LD area: WT = 0.871, KO = 0.137, \*\*P  $\leq$  0.01. The absolute changes ( $\Delta$ ) in LD number and total area from time point 0 h–12 h were evaluated. n = 3, t-test, \*P  $\leq$  0.05. (b) Confocal fluorescence live cell imaging of cells treated with BODIPY558/568 C<sub>12</sub> during EBSS treatment. Cells were preprobed with 5 nM BODIPY558/568 C<sub>12</sub> for 24 h and incubated in fresh medium for 1 h before microscopy. The depicted cells are representative for approx. 20 imaged cells per condition from three independent approaches.

triacylglycerides (TAGs) and sterol esters, which are separated from the cytosol by a phospholipid monolayer, and are coated by a distinct set of proteins [28]. Under lipolytic conditions, TAGs are hydrolyzed by the activity of various lipases and the

generated fatty acids are utilized for energy metabolism or are modified to appropriate lipids within the ER [29]. Importantly, recent studies employing yeast or human cell lines have demonstrated that specific LD-associated lipases, including PNPLA2/ATGL

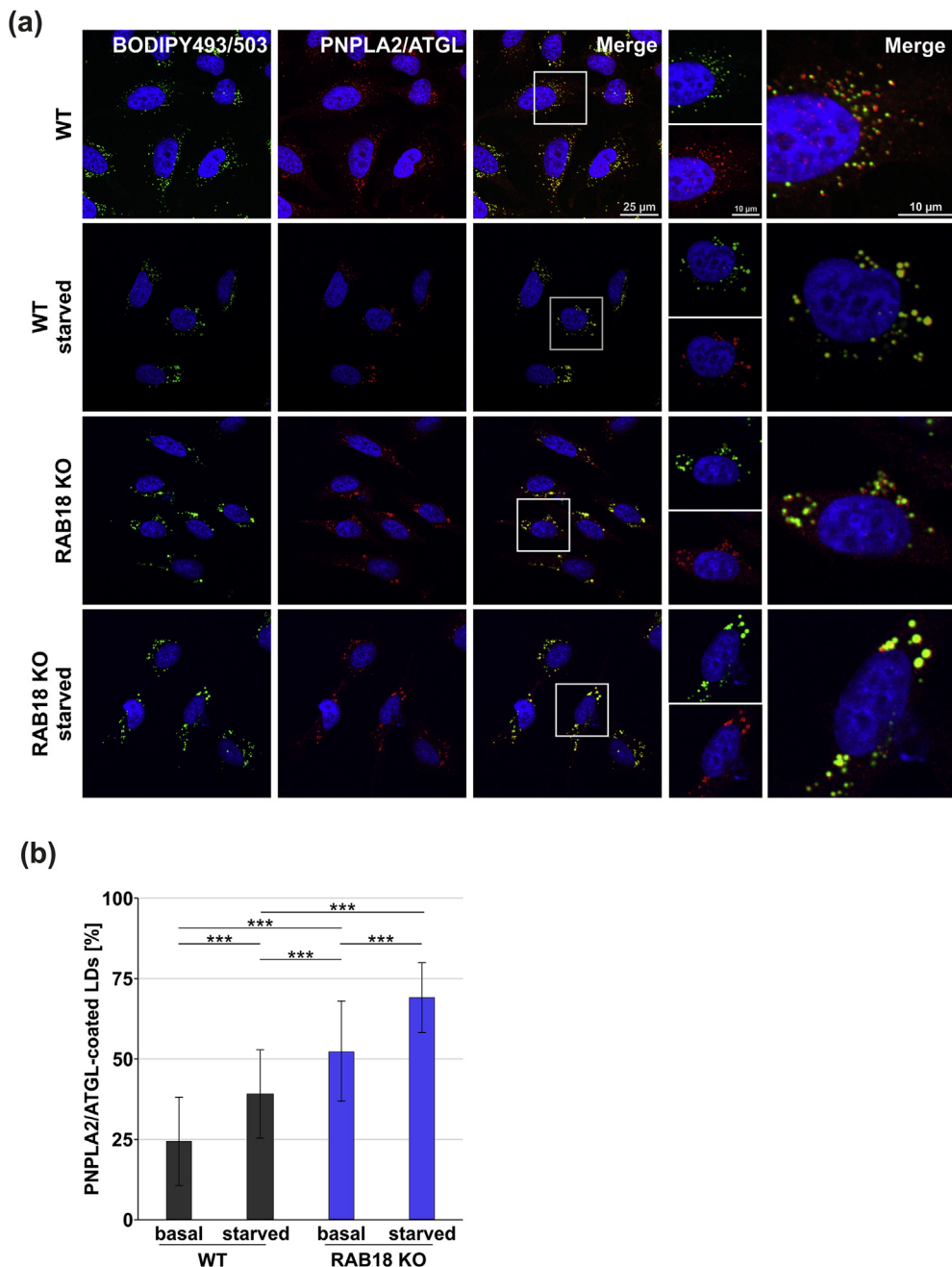


**Fig. 3. The loss of RAB18 enhances the localization of PNPLA2/ATGL at LDs.** (a) Representative confocal fluorescence images of cells stained with PNPLA2/ATGL (red), BODIPY493/503 (green), and DAPI (blue). WT cells are shown under basal and lipolytic conditions (2 h EBSS). For each condition, approx. 15 images from three independent approaches were obtained. (b) PNPLA2/ATGL colocalization with LDs under basal and lipolytic conditions (2 h EBSS) have been analyzed in approx. 45 single WT and RAB18 KO cells. Statistics are depicted as mean  $\pm$  SD. n = 3, t-test, \*\*\*P  $\leq$  0.001.

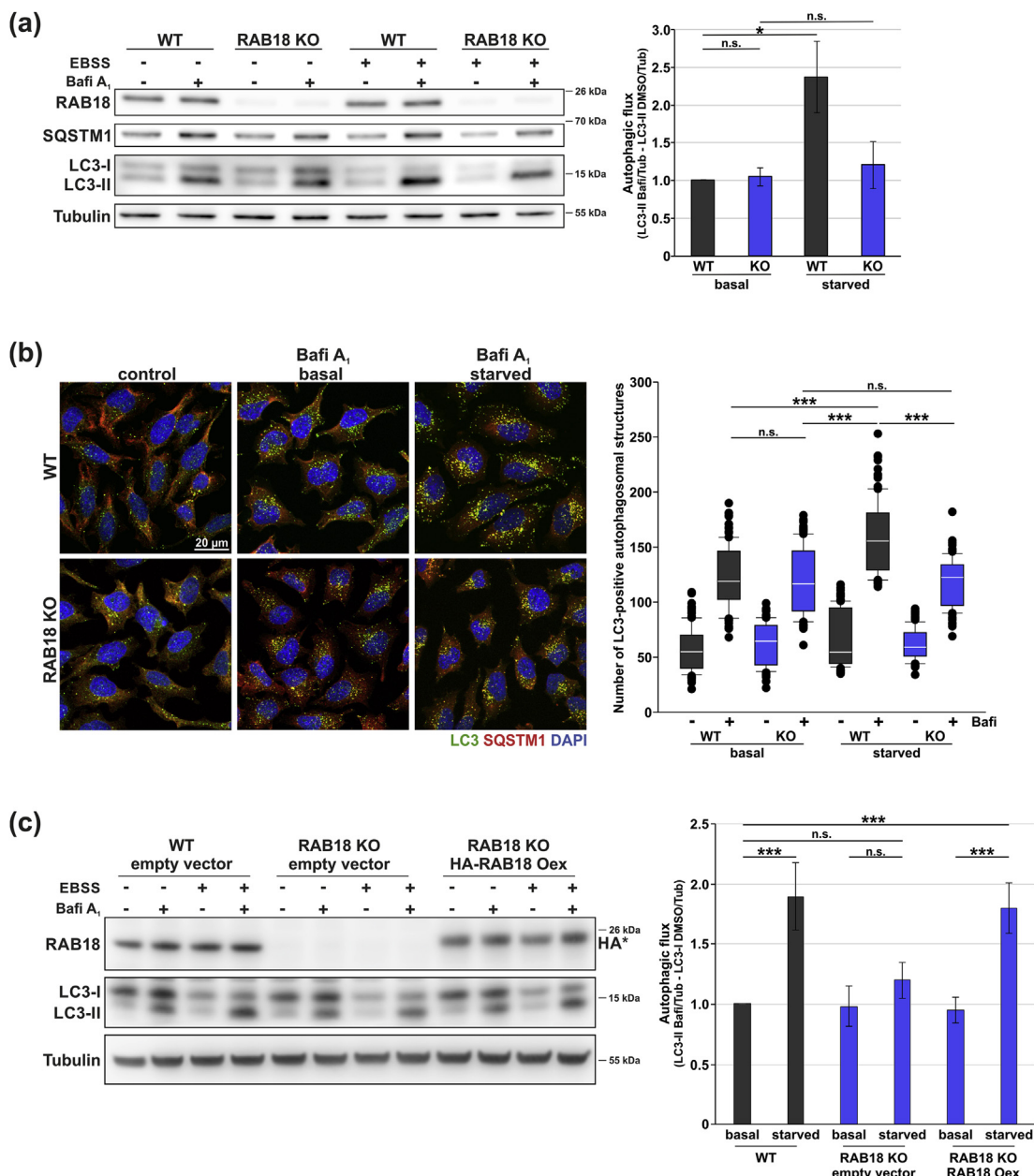


**Fig. 4. Limited lipid availability affects autophagy in RAB18 KO cells.** **(a)** Immunoblot analyses of autophagic activity under basal and induced conditions (2 h EBSS). Cells were treated with DMSO (control) or bafilomycin A<sub>1</sub> (Bafi A<sub>1</sub>) for 2 h to allow LC3-II flux evaluation. LC3-II levels were corrected over the loading control Tubulin. Statistics are depicted as mean ± SD. n = 4, One-Way ANOVA, n. s. = not significant, \*P ≤ 0.05. **(b)** Immunocytochemical stainings of LC3 (green) and SQSTM1/p62 (red). Nuclei were stained with DAPI (blue). Cells were treated with DMSO (control) or Bafi A<sub>1</sub> under basal conditions or upon EBSS treatment (2 h). For statistical analysis, autophagosomal structures (LC3) were quantified in approx. 120 single cells per cell line and condition from four independent experiments. One-Way ANOVA, n. s. = not significant, \*\*\*P ≤ 0.001. Single channels as well as quantification of SQSTM1-positive structures are presented in Supplementary Fig. 7. **(c)** Immunoblot analyses of autophagic activity upon reintroduction of RAB18 under basal and induced conditions (2 h EBSS). Cells were transfected with empty vector or HA-tagged wild-type RAB18 and were treated with DMSO (control) or Bafi A<sub>1</sub> for 2 h. LC3-II levels were corrected over Tubulin. Statistics are depicted as mean ± SD. n = 4, One-Way ANOVA, n. s. = not significant, \*\*\*P ≤ 0.001.

and PNPLA5, modulate autophagy and that LD-derived lipids support the formation of autophagosomes [15–17,30].

The RAB GTPase RAB18 has functionally been associated with LD metabolism [31] and is a positive modulator of autophagy [32]. RAB18 localizes to LDs, and this association has been linked to a function in LD biogenesis and/or consumption [31,33–35]. The interaction of RAB18 with ER-linked tethering factors mediates the connection of LDs with the ER membrane and facilitates LD maturation [35–37]. In a human mammary carcinoma cell line (SUM159), however, an involvement of RAB18 in LD metabolism could not be observed [38]. Importantly, loss-of-function mutations in *RAB18* cause Warburg Micro syndrome (WARBM) [39], a severe human autosomal recessive (neuro-)developmental disorder. The molecular basis responsible for the pathogenesis remains unclear, yet, WARBM patient cells are characterized by an altered LD homeostasis [40].

In this study, we examined the impact of RAB18 on LD metabolism and autophagy. The stable knockout of the RAB GTPase provoked an LD phenotype that resembled WARBM patient cells. In-depth analysis revealed that fatty acid release was impaired in the absence of RAB18. The resulting insufficient LD-derived lipid availability influenced autophagy, causing adaptations in the autophagy network, which included an increased expression and altered phosphorylation of ATG2B as well as augmented levels of ATG12-ATG5 conjugates. Additionally, the phosphorylation of ATG9A and its trafficking were enhanced in RAB18 KO cells under basal autophagy conditions, which supported the maintenance of autophagic activity.

Thus, we were able to directly associate the role of RAB18 in LD catabolism with autophagy and to demonstrate the significant impact of LD-derived lipids on the degradative pathway. Moreover, we characterized autophagy network adaptations that

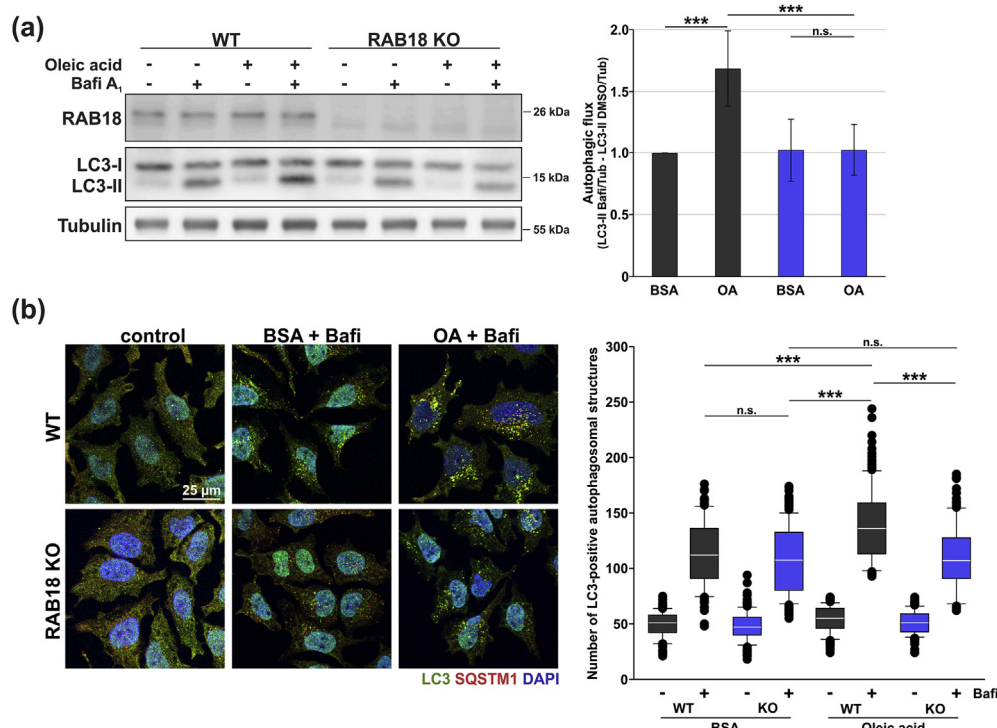
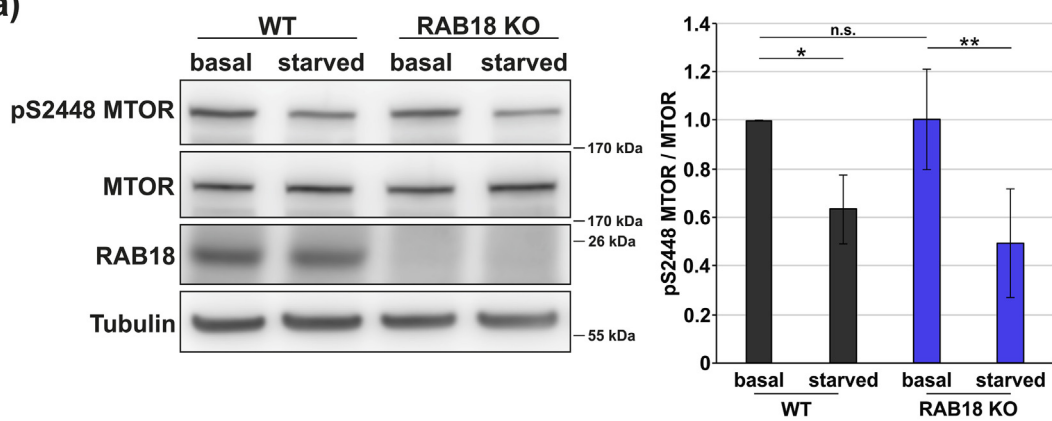
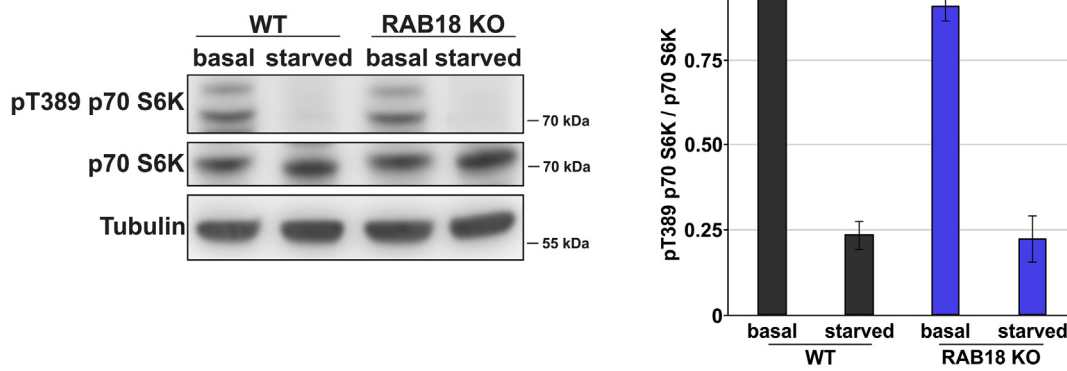


**Fig. 5. Abundant lipid availability does not affect autophagy in RAB18 KO cells.** (a) Immunoblot analyses of autophagic activity after oleic acid (OA) treatment. Cells were pretreated with BSA (control) or BSA-conjugated oleic acid and with DMSO (control) or bafilomycin A<sub>1</sub> (Bafi A<sub>1</sub>) for 3 h to allow LC3-II flux evaluation. Statistics are depicted as mean  $\pm$  SD, n = 4; One-Way ANOVA, n. s. = not significant, \*\*P  $\leq$  0.01. (b) Immunocytochemical stainings of LC3 (green) and SQSTM1 (red). Nuclei were stained with DAPI (blue). Cells were treated with DMSO (control) or Bafi A<sub>1</sub> under control conditions or upon OA treatment (2 h). Shown here are merged images, single channels are presented in Supplementary Fig. S9. For statistical analysis, autophagosomal structures (LC3) were quantified in approx. 150 single cells per cell line and condition from three independent experiments. One-Way ANOVA, n. s. = not significant, \*\*\*P  $\leq$  0.001. In Supplementary Fig. S9 SQSTM1-positive autophagosomal structures are statistically analyzed.

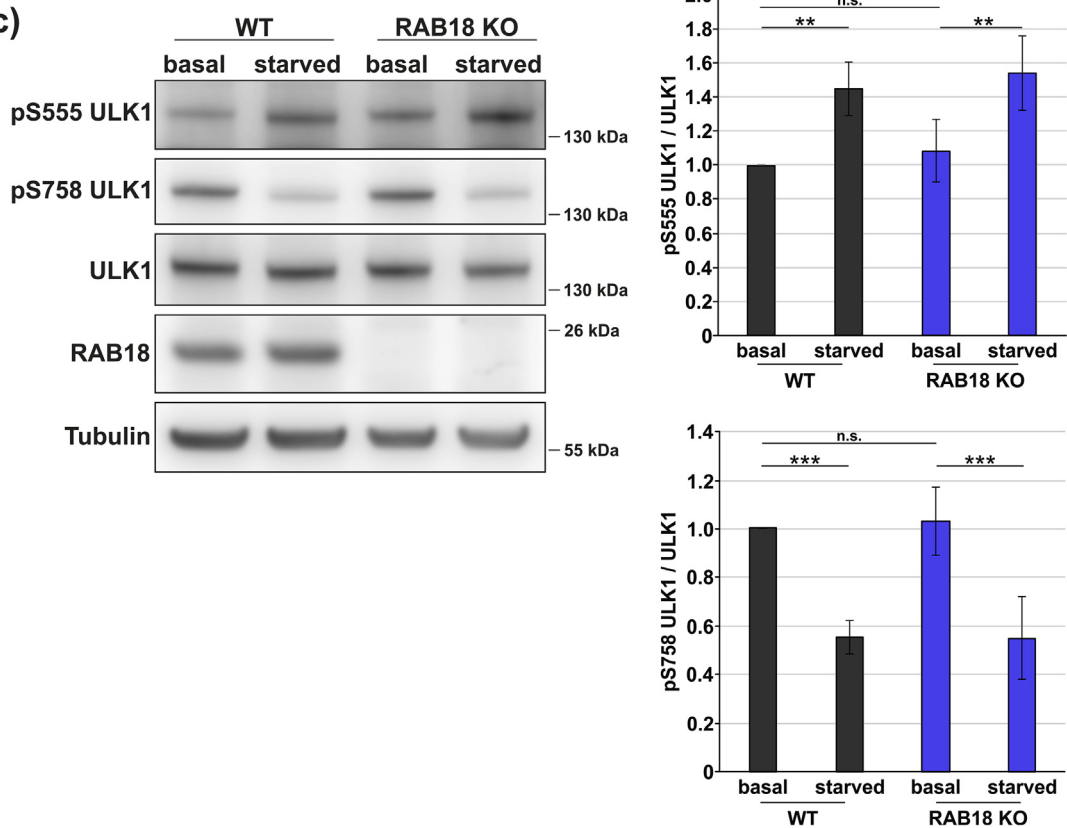
(a)



(b)



(c)



rescue basal autophagic activity under conditions of decreased lipid availability.

## Results

Previously, employing transient genetic manipulations, we have characterized RAB18 as a positive modulator of autophagy [32]. To conduct more detailed analyses on RAB18 function, we generated stable KO HeLa cells of the RAB GTPase, employing the CRISPR/Cas9 technology, and selected two independent clonal cell lines ([Supplementary Fig. S1](#)).

Initially, we focused on the impact of the RAB18 KO on LDs and visualized the lipid reservoirs with BODIPY493/503, which stains neutral lipids. Fluorescence imaging revealed a striking LD appearance in the absence of RAB18 ([Fig. 1a](#), [Supplementary Fig. 2](#)), similar to WARB patient cells [40]. LDs were reduced in number and enlarged in size and accumulated in the perinuclear region of the cell with a reduced mean distance from the nucleus when compared to HeLa wild-type (WT) cells ([Fig. 1a–d](#)). This result was further strengthened by transmission electron microscopy (TEM), showing enlarged LDs in KO cells ([Fig. 1e, f](#)), which were mostly localized close to the nucleus. Importantly, reintroducing RAB18 into the KO cells reversed the LD alterations ([Supplementary Fig. S3](#)). Overexpression of wild-type RAB18 resulted in small, dispersed LDs in WT as well as RAB18 KO cells, confirming the findings of Xu et al. [35].

Notably, the CRISPR/Cas9-mediated stable RAB3GAP1 KO caused a similar LD appearance as observed in RAB18 KO cells ([Fig. 1a](#), [Supplementary Fig. S2](#)). RAB3GAP1 functions as an upstream regulator of RAB18, acting as a RAB GEF, activating the RAB GTPase [32,35,41]. Loss-of-function mutations in *RAB3GAP1* have likewise been associated with WARB [42]. Thus, we detected an altered LD appearance in cell lines with a KO in different genes that encode functionally associated proteins, emphasizing the relevance of RAB18 and RAB3GAP1 in LD homeostasis.

Presuming that the LD phenotype originates from an altered LD metabolism, we investigated their consumption under starvation conditions. Nutrient

deprivation results in the hydrolysis of TAGs and the release of fatty acids for mitochondrial energy metabolism [43]. Indeed, starvation triggered a time-dependent reduction in LD numbers and total area in WT cells, while this process was clearly repressed in KO cells ([Fig. 2a](#)).

In order to directly investigate fatty acid release from LDs, we employed the dye-conjugated fatty acid BODIPY558/568 C<sub>12</sub> and live cell imaging, following an established method [43]. As expected, in WT cells, the fatty acid efficiently migrated out of LDs under lipolytic conditions ([Fig. 2b](#)). The LD-located fluorescence signal decreased and the area of single LDs progressively declined during the starvation period. In contrast, the fatty acid was largely immobile in KO cells, emphasizing that its mobilization is disturbed in the absence of RAB18.

One key component of LD turnover is the lipase PNPLA2/ATGL, which is responsible for the release of fatty acids from TAGs. Under lipolytic conditions, the enzyme localizes to LDs and mediates the hydrolysis of TAGs, generating diacylglycerides [44,45]. Here, we analyzed the association of PNPLA2/ATGL with LDs, employing immunocytochemistry ([Fig. 3a, b](#)). Remarkably, the lipase showed an enhanced localization at LDs in RAB18 KO cells already under basal conditions, which we observed in WT cells only after inducing lipolysis. This showed that the permanent loss of RAB18 did not affect the transfer of PNPLA2/ATGL to LDs. However, the enhanced LD localization of the lipase was not linked to an efficient fatty acid release ([Fig. 2a, b](#)), underlining the specific importance of RAB18 for LD catabolism.

The KO of RAB18 interferes with LD turnover. To investigate whether it also affects LD formation, we monitored the dynamics of LD buildup upon oleic acid supplementation ([Supplementary Fig. S4](#)). Fatty acid treatment resulted in the rapid increase in LD numbers as well as total LD area, and importantly, we observed no significant differences between WT and KO cells. This demonstrated that the induced generation of LDs was unaffected by the stable loss of RAB18. The protein BSCL2/Seipin is functionally relevant for LD biogenesis [46]. BSCL2/Seipin forms ER-LD contact sites and regulates the stable association of forming LDs with the ER, facilitating the transfer of lipid cargo and

**Fig. 6. The phospho-regulation of MTOR and ULK1 is unaffected in RAB18 KO cells.** (a) Immunoblot analyses of MTOR levels and phosphorylation of residue S2448 under basal and starved conditions (2 h EBSS). Statistics are depicted as mean  $\pm$  SD. n = 4, One-Way ANOVA, n. s. = not significant, \*P ≤ 0.05, \*\*P ≤ 0.01. Statistical analysis of total MTOR levels is shown in [Supplementary Fig. S10](#). (b) Immunoblot analyses of p70 S6K levels and phosphorylation of T389 under basal and starved conditions (2 h EBSS). Statistics are depicted as mean  $\pm$  SD. n = 4, One-Way ANOVA, n. s. = not significant, \*\*P ≤ 0.01. (c) Immunoblot analyses of ULK1 levels and phosphorylation of residues S555 and S758 under basal and starved conditions (2 h EBSS). Statistics are depicted as mean  $\pm$  SD. n = 4, One-Way ANOVA, n. s. = not significant, \*\*P ≤ 0.01, \*\*\*P ≤ 0.001. Statistical analysis of total ULK1 levels is shown in [Supplementary Fig. S10](#).

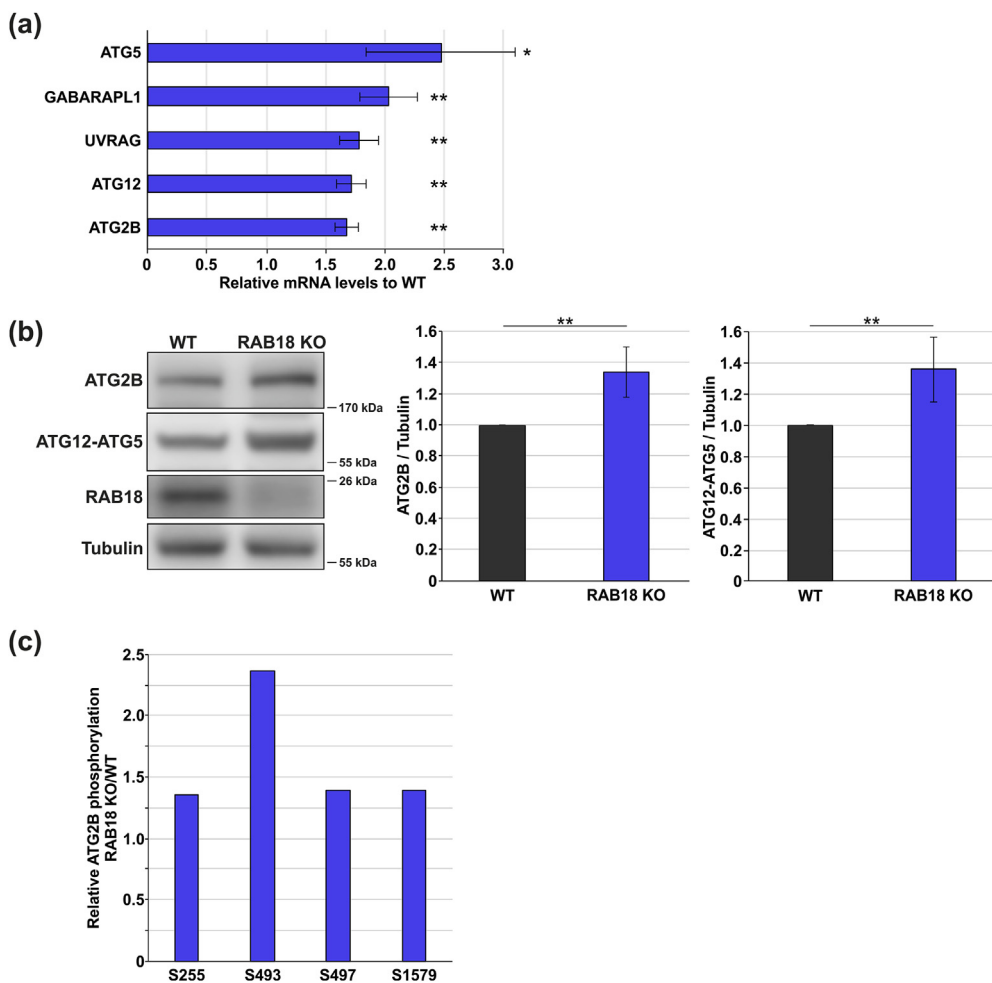


**Fig. 7. Autophagy network alterations in RAB18 KO cells.** (a) Genes showing altered expression levels in RAB18 KO compared to WT cells as evaluated using the qPCR array ([Supplementary Table 2](#)). mRNA levels were evaluated in relation to the respective levels in WT cells and the threshold for upregulation was set to 1.5-fold. n = 3, t-test, \*P ≤ 0.05, \*\*P ≤ 0.01. (b) Immunoblot analyses of ATG2B protein and ATG12-ATG5 conjugate levels in WT and RAB18 KO cells. Statistics are depicted as mean ± SD. n = 4, t-test, \*\*P ≤ 0.01. (c) Phosphorylation levels of ATG2B (Q96BY7) serine residues in RAB18 KO compared to WT cells, determined by SILAC-based phosphoproteomics and depicted as mean values of two replicates.

proteins [47]. To further support the finding that LD formation is indeed unaffected in RAB18 KO cells, we investigated the localization of BSCL2/Seipin and observed no difference comparing WT and KO cells ([Supplementary Fig. S5](#)). The ER-located protein closely associated with small LDs upon conditions preferring LD formation. Thus, in contrast to LD consumption, we gained no indication that the biogenesis of the lipid reservoirs was affected by RAB18 loss.

Next, we analyzed the influence of alterations in LD turnover on autophagy, considering that autophagosome synthesis is strongly dependent on a sufficient lipid supply. In contrast to our previous findings analyzing transient genetic manipulations of RAB18 [32], here, using stable RAB18 KO cells, we

found that basal autophagic activity was actually unaffected ([Fig. 4](#)). In fact, immunoblot analyses of the lipidated LC3-II showed no differences when comparing WT and KO cells under basal, uninduced, autophagy conditions ([Fig. 4a](#), [Supplementary Fig. S6a](#)). This result was confirmed by confocal fluorescence microscopy of LC3- and SQSTM1-positive autophagosomes ([Fig. 4b](#), [Supplementary Figs. S7a, b](#)). The amount of LC3- as well as SQSTM1-positive autophagosomal structures and their baflomycin A<sub>1</sub>-mediated accumulation was comparable in WT and KO cells under basal autophagy conditions.

Intriguingly, starvation increased autophagic activity in WT cells as expected; however, it failed to induce autophagy in RAB18 KO cells ([Fig. 4a, b](#),

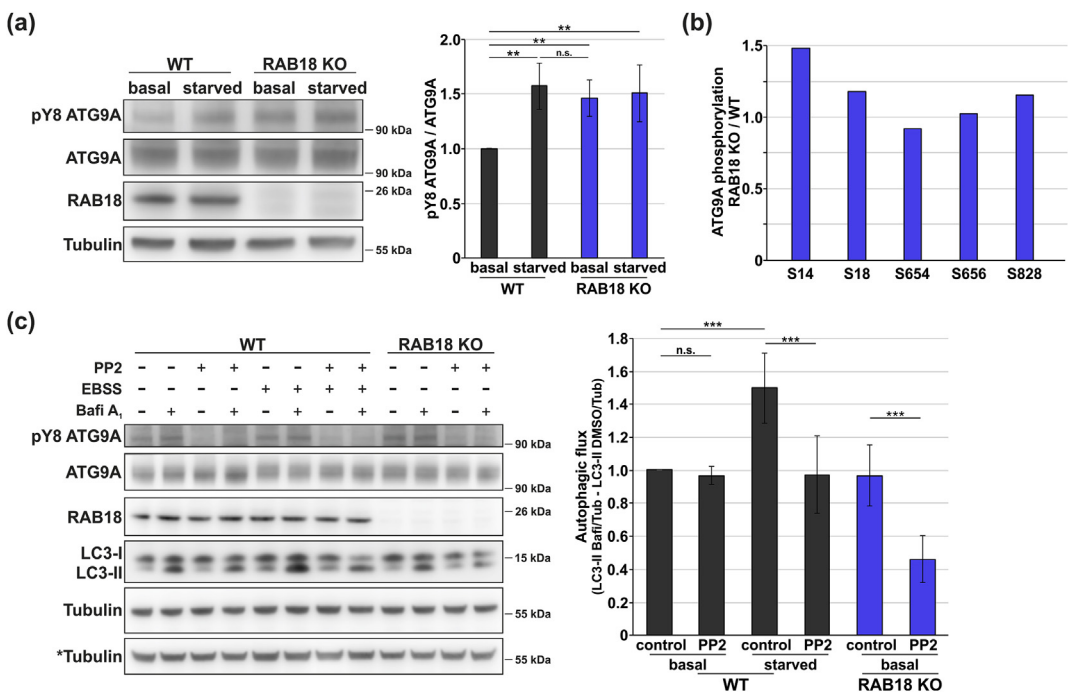


**Fig. 8. ATG9A phosphorylation is altered in RAB18 KO cells and impacts autophagy.** (a) Immunoblot analyses of Y8 phosphorylation of ATG9A in RAB18 KO and WT cells under basal and starved conditions (2 h EBSS). Statistics are depicted as mean  $\pm$  SD. n = 4, One-Way ANOVA, n. s. = not significant, \*\*P  $\leq$  0.01. (b) Phospho-levels of serine residues of ATG9A (Q7Z3C6) in RAB18 KO compared to WT cells, determined by SILAC-based phosphoproteomics and depicted as mean values of two replicates. (c) Immunoblot analyses of autophagic activity upon SRC kinase inhibition via PP2 treatment (5  $\mu$ M for 12 h). WT cells were examined under basal and starved conditions (2 h EBSS). All cells were treated with DMSO (control) or baflomycin A<sub>1</sub> (Baf A<sub>1</sub>) for 2 h to allow evaluation of LC3-II flux. LC3-II loading was corrected over Tubulin. \*indicates Tubulin loading control corresponding to parallel ATG9A blot. Statistical analyses are depicted as mean  $\pm$  SD. n = 5, One-Way ANOVA, n. s. = not significant, \*\*\*P  $\leq$  0.001.

**Supplementary Figs. S6a, S7a, b:** immunoblotting as well as immunocytochemical analyses of autophasosomal structures showed that the KO cells did not respond to nutrient deprivation with the usually observed increased autophagic activity. Notably, we confirmed these findings in RAB3GAP1 KO cells (**Supplementary Fig. S8**). The stable loss of RAB3-GAP1 had no impact on basal autophagic activity, but impeded the induction-mediated increased autophagic flux.

Again, as observed for LDs, reintroduction of RAB18 restored the KO effect (Fig. 4c, Supplementary Fig. S6b). Expression of wild-type RAB18 facilitated autophagy induction upon starvation and resulted in increased autophagic activity, emphasizing the direct relevance of RAB18 function for the detected alterations.

RAB18 KO cells are characterized by reduced fatty acid release from LDs (Figs. 1–3), which might result in an insufficient lipid supply for autophagosome formation. To analyze the significance of LD-derived lipids for autophagy, we investigated autophagic activity after treatment with oleic acid, in accordance with a previous study [15]. The

enhanced availability of LD-derived lipids stimulated autophagy in WT cells and facilitated the flux of LC3-II as shown by immunoblotting as well as immuno-cytochemistry (Fig. 5a, b, Supplementary Figs. S9a, b). Strikingly, in RAB18 KO cells, the treatment with oleic acid did not result in an increased autophagic activity. This data again indicates that the fatty acid transfer from LDs to the autophagic pathway is disturbed when RAB18 is absent and clearly accentuates the relevance of LD-derived lipids for autophagy.

Interestingly, in contrast to induced autophagy as well as our previous transient genetic manipulations [32], basal autophagic rates were unaffected in stable RAB18 KO cells. This indicated that the autophagy network adapted to compensate the reduced LD-derived lipid availability to maintain basal autophagic activity. In order to analyze these adaptive adjustments, we investigated the canonical autophagy induction system and analyzed phosphoregulations of the kinases MTOR and ULK1.

MTOR is regulated via phosphorylation at multiple sites, and we focused on amino acid residue S2448 [48]. Interestingly, we found no differences in its

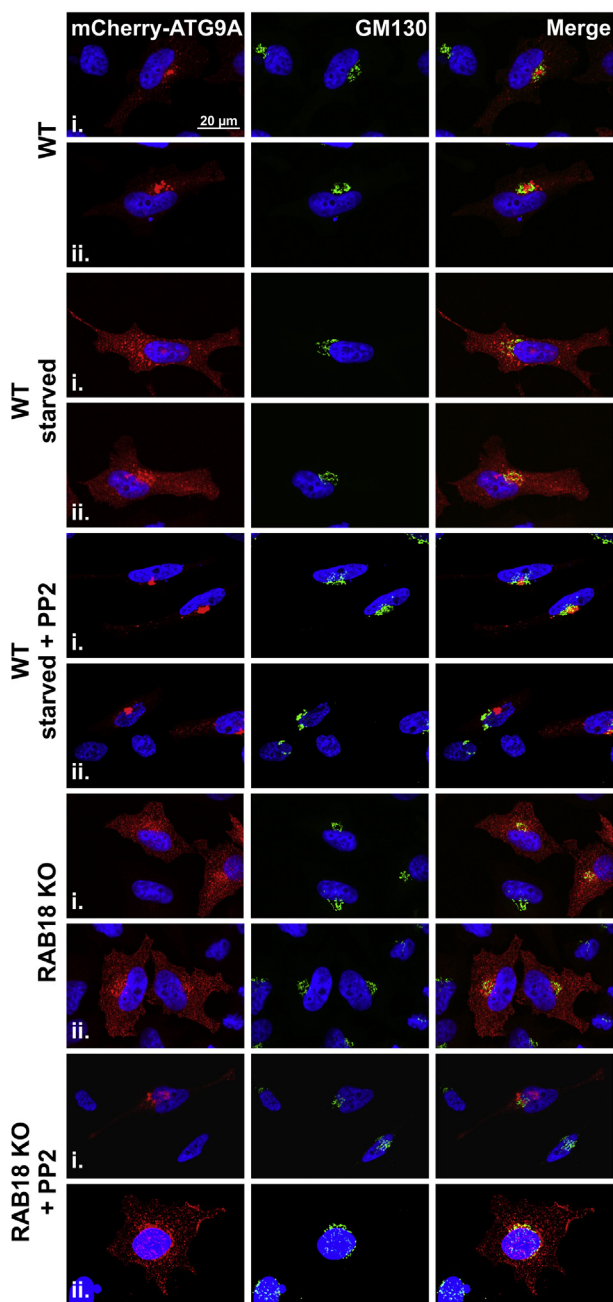


**Fig. 9. ATG9A trafficking dynamics are enhanced under basal conditions in RAB18 KO cells.** Representative confocal fluorescence images of cells expressing mCherry-ATG9A (red), stained with GM130 (Golgi, green), and DAPI (nuclei, blue). Cells were examined under basal conditions, upon starvation (2 h EBSS), and/or upon PP2 treatment (5  $\mu$ M for 8 h). Approx. 20 images for each condition were obtained from three independent experiments.

starvation-mediated phosphorylation as well as in total MTOR protein levels when comparing KO and WT cells (Fig. 6a, Supplementary Fig. S10). Additionally, we examined the phosphorylation of the MTOR substrate p70 S6 kinase at amino acid residue T389 and found no differences in its phospho-levels under basal conditions and upon starvation (Fig. 6b). Thus, the loss of RAB18 had no impact on the activity of MTOR kinase. ULK1 activity is modulated via several phosphorylations upon starvation, and we examined the MTOR-mediated, inactivating, phosphorylation at S758 as well as the AMP kinase PRKAA1-mediated, activating, phosphorylation at S555 [49,50]. Importantly, both regulations as well as total ULK1 protein levels were comparable in KO and WT cells (Fig. 6c, Supplementary Fig. S10). Thus, MTOR and ULK1 phosphoregulations were unaffected by the RAB18 KO, demonstrating that the adaptations of the autophagy network were not linked to modifications in canonical autophagy induction. In addition, we conducted a SILAC-based quantitative phosphoproteomics approach, which confirmed that the phospho-levels of these amino acid residues were unaltered when comparing KO and WT cells, while other residues showed alterations under basal conditions (Supplementary Table S1, Supplementary Fig. S11).

Next, we investigated direct modifications of the autophagy network in RAB18 KO cells and analyzed expression levels of key autophagy proteins employing a qPCR array (Fig. 7a, Supplementary Table S2). Interestingly, mRNA levels of a discrete number of autophagy factors were upregulated in KO cells, whereas actually no downregulations were observed. This underlines the positive adaptation of the autophagy network with the aim to rescue the activity of the degradative pathway under unfavorable conditions. Remarkably, all regulated proteins can be allocated to early steps of the autophagy process, suggesting that the network responded to the stable RAB18 loss with alterations that facilitate autophagosome formation. In fact, expression levels of ATG2B as well as ATG5 and ATG12 were enhanced in RAB18 KO cells, and importantly, this directly correlated with increased ATG2B protein and ATG12-ATG5 conjugate levels when compared to WT cells (Fig. 7b).

Combined findings from the SILAC-based phosphoproteomics approach and the expression analysis underline the particular regulation of ATG2B. In RAB18 KO cells, in addition to the increased expression levels, ATG2B showed an enhanced phosphorylation of the particular amino acid residue S493 (Fig. 7c, Supplementary Fig. S11, Supplementary Table S1). Since ATG2 proteins have recently been described as lipid transfer factors that promote autophagosome formation [51,52], the detected regulation of ATG2B emphasizes that adaptational autophagy network alterations are specifically

targeted and include distinct factors related to autophagosome formation and potentially lipid transfer.

Within the autophagy network, ATG9A is well acknowledged to function in the transfer of vesicles from the cellular periphery to the site of autophagosome formation to supply required proteins as well as lipids [22,24,25]. Thus, the protein is indeed an important candidate to compensate reduced LD-derived lipid availability. Notably, mRNA and protein levels of ATG9A were not altered in RAB18 KO cells (Supplementary Fig. S12). However, the activity of ATG9A is regulated via phosphorylation at amino acid residues Y8 and S14, which direct the protein to the autophagy pathway and facilitate autophagosome formation [26,27]. We analyzed the phospho-status of the Y8 residue by immunoblotting and found that its phosphorylation levels were enhanced in RAB18 KO cells already under basal autophagy conditions, which we observed in WT cells solely upon induction (Fig. 8a). Again, this data point was confirmed in RAB3GAP1 KO cells, which showed basally enhanced Y8 phosphorylation (Supplementary Fig. S13).

Due to the lack of a specific antibody directed against the phosphorylated S14 residue, we employed the quantitative phosphoproteomics approach to analyze S14 phosphorylation levels and found that they were in fact slightly, but reproducibly, enhanced in RAB18 KO cells (Fig. 8b, Supplementary Fig. S11, Supplementary Table S1). Since the phosphoproteomics exclusively detected the serine residues on ATG9A, confirmation for Y8 by this approach was not possible.

Y8 phosphorylation of ATG9A is mediated by SRC kinase [27]. To confirm this link and to gain insight into the functional importance of this ATG9A modification, we employed the two SRC kinase inhibitors PP2 (Fig. 8c) and SU6656 (Supplementary Fig. S14). Indeed, SRC kinase inhibition impeded the autophagy induction mediated increased Y8 phosphorylation in WT cells and prevented induced autophagic activity. Importantly, basal autophagic flux was not significantly affected by SRC kinase inhibition in WT cells. Remarkably, in contrast to WT cells, the decreased Y8 phosphorylation by PP2 as well as SU6656 treatment in RAB18 KO cells resulted in reduced autophagic activity already under basal conditions (Fig. 8c, Supplementary Fig. S14). These findings demonstrate that ATG9A phosphorylation supports the maintenance of basal autophagy in the absence of RAB18.

RAB18 has been shown to affect the function of the Golgi complex [53], which is also a central compartment for ATG9A trafficking. To exclude that phosphorylation of ATG9A is related to functional perturbations of the Golgi, we disrupted its function

and monitored the impact on Y8 phospho-levels by immunoblotting (Supplementary Figs. S15a, b). The treatment with golgicide did not result in enhanced Y8 phosphorylation.

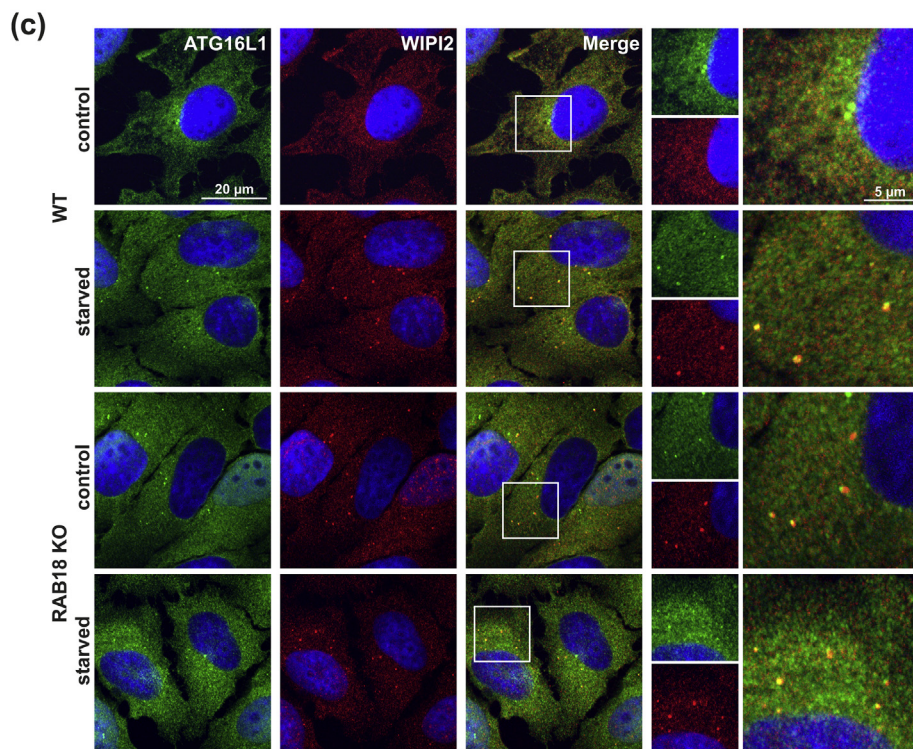
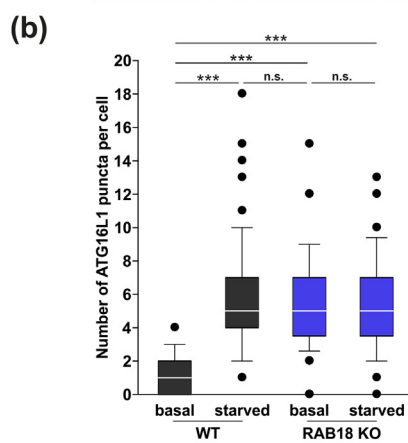
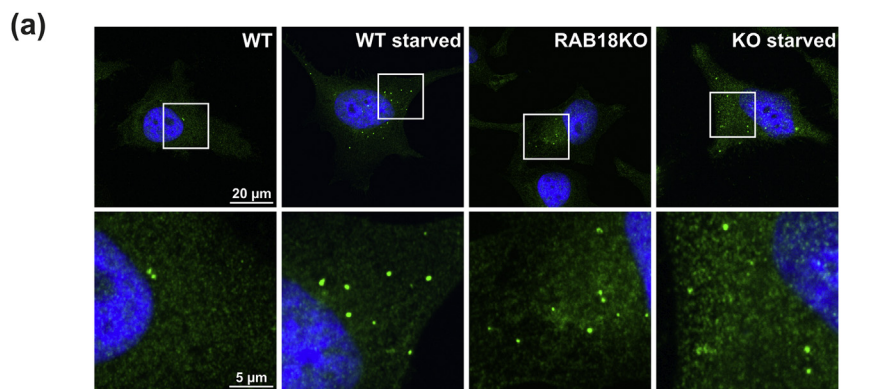
In order to conduct a more detailed investigation into ATG9A dynamics in RAB18 KO cells, we directly analyzed ATG9A trafficking. The protein prominently localizes to the Golgi complex under basal autophagy conditions and changes to a dispersed vesicular distribution upon autophagy induction [23,25]. Employing immunocytochemistry, we analyzed the localization of ATG9A in WT and KO cells (Fig. 9). As expected, the majority of ATG9A was located at the Golgi in WT cells, but changed to a dispersed distribution upon starvation-mediated autophagy induction. Remarkably, in RAB18 KO cells, ATG9A showed the dispersed vesicular distribution already under basal conditions, which is directly related to the observed enhanced phosphorylation. Inhibition of SRC kinase activity affected ATG9A trafficking. The treatment with PP2 reversed the dispersed appearance and resulted in enhanced localization of ATG9A at the Golgi in KO cells under basal conditions as well as in WT cells upon starvation. This indicates an important role of Y8 phosphorylation for ATG9A trafficking dynamics and emphasizes the relevance of this particular modification in RAB18 KO cells.

Autophagy induction and dynamic ATG9A trafficking are associated with the increased appearance of ATG16L1-positive pre-autophagosomal structures. ATG16L1 is targeted to the phagophore, where it forms a complex with the ATG12-ATG5 conjugate, which is required for the lipidation of Atg8 family members [9,11,12]. In fact, starvation resulted in increased numbers of ATG16L1 puncta in WT cells, which were already observed in RAB18 KO cells under basal conditions (Fig. 10a, b). Importantly, these ATG16L1 puncta were also positive for WIPI2 (Fig. 10c). Upon autophagy induction, WIPI2 is recruited to the omegasome at the ER and remains associated with the growing phagophore, where it is essential for the recruitment of ATG16L1 [8].

Thus, the comparison of WT cells upon autophagy induction to RAB18 KO cells under basal conditions showed similar ATG9A trafficking and an enhanced presence of ATG16L1 as well as WIPI2-positive phagophore structures. This further demonstrated that ATG9A activity is increased in RAB18 KO cells, facilitating basal autophagic activity under lipid-limited conditions.

## Discussion

In the present study, we connect the impact of RAB18 on LD catabolism with autophagy. The stable



loss of RAB18 results in a reduced LD-derived lipid availability that provokes adaptive alterations of the autophagy network to maintain autophagic activity.

RAB18 has been implicated to function in a broad range of cellular processes, including LD homeostasis [54]. However, its exact role in LDs metabolism remains indistinct. Recent studies range from functionally linking RAB18 to ER-LD tethering, to LD maturation, or to no influence on LD turnover at all [31,33–38]. Here, we show that the stable loss of RAB18 results in functionally inert LDs. The lipid reservoirs are efficiently formed but the fatty acid release on demand is impeded, despite an enhanced localization of the TAG lipase PNPLA2/ATGL at the organelles. Previous studies showed that modulating PNPLA2/ATGL levels reciprocally affects the number of LDs in HeLa cells [55] and that the LD association and activity of the lipase are dynamically regulated [56,57]. Thus, the detailed functional correlation of PNPLA2/ATGL activity and the permanent loss of RAB18 requires further elucidation.

In conclusion, our analyses demonstrate that the stable loss of RAB18 causes a defect in LD catabolism, provoking the prominent LD appearance that, excitingly, is also observed in WARB patient cells carrying loss-of-function mutations in *RAB18* or *RAB3GAP1* [40]. Importantly, the loss of RAB3-GAP1, which is a regulator of RAB18 activity [32,41], results in a similar LD phenotype, emphasizing the relevance of RAB18 function in LD consumption.

The disturbed LD catabolism affects autophagy, which is dependent on an adequate lipid supply to guarantee sufficient autophagosome formation [3,58]. Different cellular organelles and compartments have been recognized as lipid donors [3,14]. However, the specific regulation of autophagosomal lipid acquisition remains elusive. Previous studies have demonstrated a link between LDs and autophagy [15–17], but the functional impact and importance of LD-derived lipids on autophagosome biogenesis have been questioned [18]. It has already been demonstrated that the increased availability of fatty acids from LDs enhances autophagic capacity by facilitating autophagosome formation and, importantly, that this process is dependent on LD-located lipases [15]. Fatty acids are mobilized from LDs and converted into appropriate lipids that are potentially delivered to the site of autophagosome formation.

Here, we confirm that fatty acid supplementation increases autophagic capacity in WT cells. In contrast, the enhanced fatty acid availability does not stimulate autophagy in RAB18 KO cells, demonstrating that in the absence of RAB18 their efficient transfer to the autophagy pathway is impeded, consequently affecting the degradative pathway.

Previously, employing transient genetic manipulations, we have characterized RAB18 and RAB3-GAP1 as positive modulators of autophagy [32,59]. The siRNA-mediated transient reduction of RAB18 or RAB3GAP1 levels cause a decline in autophagic activity, notably, under basal as well as induced autophagy conditions. Excitingly, as demonstrated here, the stable KO of RAB18 (as well as RAB3-GAP1) showed no impact on basal autophagic activity. The flux of LC3-II and the ratio of LC3-II to LC3-I were unaffected. However, autophagy induction, which is associated with an increased lipid demand, indeed failed. These findings indicate that the stable loss of RAB18 function leads to adaptations of the autophagy network, which rescue basal autophagy under conditions of reduced LD-derived lipid availability but are insufficient to enable an increased autophagic activity upon induction.

Indeed, we detected several alterations within the autophagy network, including increased ATG12-ATG5 conjugate and ATG2B levels. These modifications appeared already under basal autophagy conditions in RAB18 KO cells and occurred independently of the autophagy induction system, since the starvation-mediated phospho-regulation and activity of MTOR as well as ULK1 were unaffected.

ATG12 and ATG5 are covalently linked by an ubiquitin-like conjugation process, which is a prerequisite for the formation of the ATG12-ATG5/ATG16L1 complex that is required for the lipidation of Atg8 family members [11,60]. In the absence of ATG5, phagophores are formed but do not mature into fully closed autophagosomes [61,62]. Enhanced ATG5 levels facilitate autophagy; augmented conjugate levels have been linked to increased autophagic activity [63].

The increased protein levels and altered phosphorylation of ATG2B are of particular interest here. Mammalian cells possess two functionally similar ATG2 proteins, ATG2A and ATG2B, which have recently been characterized as lipid transfer factors that support phagophore growth and

**Fig. 10. ATG16L1 puncta accumulate under basal conditions in RAB18 KO cells and colocalize with WIPI2.** (a) Representative confocal fluorescence images of cells stained with ATG16L1 (green) and DAPI (blue). WT cells were examined under basal and starved conditions (2 h EBSS). (b) Statistical evaluation of (a). Approx. 65 cells for each condition from four independent experiments were analyzed and the total number of ATG16L1 puncta was quantified per cell. One-Way ANOVA, n. s. = not significant, \*\*\*P < 0.001. (c) Representative confocal images of immunocytochemical stainings using ATG16L1 (green) and WIPI2 (red). Nuclei were stained with DAPI (blue). Cells were examined under basal conditions and upon starvation (2 h EBSS). Approx. 15 images for each condition were obtained from three independent experiments.

autophagosome closure [51,52,64,65]. Noteworthy, ATG2A/B localize to phagophores as well as LDs and their transient knockdown results in the accumulation of enlarged LDs [64,66]. This indicates that ATG2A/B may be linking LD metabolism and autophagy. We presume that the upregulation of ATG2B expression observed here, together with the enhanced S493 phosphorylation, which has not been functionally characterized yet, is a direct adaptive response to the limited lipid availability.

A further adaptation of the autophagy network we identified is the phosphorylation-dependent increased ATG9A activity, which proved to be important for the maintenance of basal autophagy in RAB18 KO cells. The transmembrane protein transfers vesicles from the cellular periphery to the site of autophagosome formation, delivering proteins and lipids required for the generation of autophagic vesicles [20,22–25]. Therefore, ATG9A is indeed a prime candidate to compensate insufficient lipid availability for autophagosome formation. The activity of ATG9A is regulated by ULK1 and SRC kinase-mediated phosphorylation at amino acid residues S14 and Y8, respectively [26,27]. Both modifications are described to be enhanced upon autophagy induction, which we confirmed here for HeLa WT cells. Importantly, in RAB18 KO cells, the phosphorylation of both residues was increased already under basal, unstimulated, autophagy conditions, indicating that the activity of ATG9A adapted to compensate the reduced LD-derived lipid availability in the absence of RAB18. Indeed, ATG9A showed an enhanced trafficking that was accompanied by increased amounts of ATG16L1 and WIPI2-positive preautophagosomal structures. The pharmacological inhibition of Y8 phosphorylation demonstrated a functional relevance of this ATG9A modification for the maintenance of basal autophagy: reducing Y8 phosphorylation in RAB18 KO cells impeded ATG9A trafficking dynamics and caused a clear decline in autophagic activity already under basal autophagy conditions. Thus, here, we describe the phosphorylation-dependent activation of ATG9A as a cellular adaptation aiming to compensate limited lipid availability and supporting the maintenance of autophagic activity.

In summary, we define the molecular function of RAB18 in connecting LD catabolism and autophagy and emphasize the high-impact role of LDs as lipid sources for autophagosome formation. The loss of RAB18 results in a reduced LD-derived lipid availability that provokes autophagy network adaptations, which reflect changes normally only observed upon autophagy induction, aiming to maintain autophagic activity. Thus, we uncover an exciting autophagy network plasticity, which ensures basal autophagic efficacy under unfavorable—here lipid-limiting—conditions.

## Materials and Methods

### Cell culture

HeLa cells were cultured in DMEM, supplemented with 10% fetal bovine serum, 1 mM sodium pyruvate, and 1 × antibiotic-antimycotic solution at 37 °C in a 5% CO<sub>2</sub>-humidified atmosphere. Cell identity was authenticated via STR analysis and cells were regularly tested negative for the presence of mycoplasma using the Venor GeM Mycoplasma PCR detection kit (Minerva Biolabs, 11-1050). Stock solutions of bafilomycin A<sub>1</sub> (Biozol, TRC-B110000) and rapamycin (Enzo, BML-A275-0025) were prepared in DMSO and employed as described before [59]. Stock solutions of PP2 (Sigma Aldrich, P0042) and SU6656 SRC Inhibitor (Selleck Chemicals, S7774) were prepared in DMSO and cells were treated with 5 μM and 10 μM, respectively, for 8 h (immunocytochemistry) or 12 h (immunoblotting). Cells were transfected with 30 μg of mCherry-ATG9A plasmid and transfections were carried out by electroporation as described previously [59].

### CRISPR/Cas9-mediated knockout

Gene-specific CRISPR/Cas9 vectors (pLV-U6g-EPCG) targeting *RAB18* and *RAB3GAP1* were obtained from Sigma Aldrich. Wild-type HeLa cells were transfected with 15 μg of plasmids, and selection of positive clones was performed using culture medium containing 1 μg/ml puromycin. Positive knockout clones were identified via immunoblotting and qPCR.

### Immunoblotting

Immunoblot analyses were performed as previously described [32]. Usually 15–30 μg of total protein was subjected to hand-cast 12% Bis-Tris or 4–12% NuPage Bis-Tris gels (Thermo Scientific, MP0335) and transferred onto nitrocellulose membranes. Membranes were blocked with 5% milk powder in TBS-Tween 20 and probed with the appropriate primary and secondary antibodies. Proteins were detected by chemiluminescence and developed using the Amersham Imager 600 (GE Healthcare Life Science). Primary antibodies: MAP1LC3B (Sigma, L7543), SQSTM1 (Progen, GP62-C), RAB18 (Proteintech, 11304-1-AP), RAB18 (Santa Cruz Biotechnology, sc-393168), RAB3GAP1 (Sigma, SAB4500914), RAB3GAP2 (Sigma, HPA026273), Tubulin (Sigma, T9026), ATG2B (abcam, ab116215), ATG5 (Novus, NB110-53818), ATG9A (Cell Signaling, 135095), p-Y8-AT9A (kindly provided by Yushan Zhu and Quan Chen, Nankai, China, or, alternatively, obtained from Proteintech), ULK1 (Cell Signaling, 8054), p-ULK1 Ser555 (Cell Signaling, 5869), p-ULK1 Ser757 (Cell Signaling, 6888), mTOR (Cell Signaling, 2972S), p-mTOR S2448 (Cell Signaling, 2971), p70 S6 kinase (Cell Signaling, 9202), p-p70 S6 kinase Thr389 (Cell Signaling, 9206).

## Immunocytochemistry

Immunocytochemistry was performed as previously described [32]. Briefly, cells were grown on glass cover slips, fixed with 4% PFA, and were permeabilized in 90% methanol, 0.02% Triton X-100, or 0.01% Saponin. Unspecific binding sites were blocked with 3% BSA in PBS. Cells were incubated with primary antibodies and fluorophore-conjugated secondary antibodies followed by DAPI. Primary antibodies: ATGL/PNPLA2 (Cell Signaling, 2138), ATG16L1 (MBL, PM040), CLIMP63 (Enzo, ENZ-ABS660), GM130 (BD biosciences, 610823), MAP1LC3B (nano Tools, 0260-100), BSCL2/Seipin (Thermo Fisher, PAS-47922), SQSTM1 (Progen, GP62-C), Tubulin (Sigma, T9026), WIPI2 (Millipore, MABC91). Stock solutions of BODIPY493/503 (Thermo Fisher, D3922) and BODIPY558/568 C<sub>12</sub> (Thermo Fisher, D3835) were prepared according to the supplier. Cells were imaged using the laser scanning microscope LSM710 (Zeiss). Live cell imaging and imaging of autophagosomal structures for quantification were performed via the Opera Phenix High-Content Screening System (Perkin-Elmer).

## Lipid droplet analysis

For LD analyses, cells were stained with Tubulin  $\alpha$ , DAPI, and BODIPY493/503 and were imaged via the Opera Phenix High-Content Screening System (Perkin-Elmer). Single cells and cell area were defined via DAPI and Tubulin  $\alpha$  staining, respectively. LD number and size were quantified through BODIPY493/503 fluorescence, employing Harmony High-Content Imaging and Analysis software (Perkin-Elmer). Distance analyses as well as PNPLA2/ATGL colocalization were conducted with ImageJ plugin DiAna [67].

## Autophagic activity analysis

Autophagic activity was analyzed in accordance with "Guidelines for the use and interpretation of assays for monitoring autophagy" [68]. Cells were treated with baflomycin A<sub>1</sub> for 2–4 h or DMSO for control and the flux of autophagic substrates was calculated by the subtraction of accumulated levels upon baflomycin A<sub>1</sub> treatment and DMSO control after correction of equal loading using Tubulin. Additionally, the ratio of LC3-II to LC3-I was calculated.

## Quantitative real-time PCR

RNA extraction, reverse transcription, and real-time PCR were performed as described previously [59]. Primer sequences for the autophagy array are listed in Supplementary Table 2.

## Transmission electron microscopy

For transmission electron microscopy, cells were grown on 7.8 mm thick Aclar discs (Ted Pella Inc.) and fixed by 2.5% glutaraldehyde in 0.1 M sodium cacodylate buffer pH 7.4. Discs were washed in 0.1 M cacodylate buffer. After

treatment with 1% OsO<sub>4</sub>, the sections were stained with uranyl acetate, dehydrated, and flat-embedded in epon resin (Araldite 502). 35 nm ultrathin cross sections were cut using an Ultracut S ultramicrotome (Reichert) and analyzed using a CM12 TEM (Philips) operated at 80 kV and equipped with an ES500W Erlangshen (782) CCD camera (Gatan).

## Quantitative phosphoproteome analysis

Quantitative phosphoproteome analysis was performed as described previously [69]. Briefly, cells were cultured in SILAC media containing L-arginine and L-lysine, L-arginine [<sup>13</sup>C<sub>6</sub>] and L-Lysine [<sup>2</sup>H<sub>4</sub>], or L-arginine [<sup>13</sup>C<sub>6</sub>–<sup>15</sup>N<sub>4</sub>] and L-lysine [<sup>13</sup>C<sub>6</sub>–<sup>15</sup>N<sub>2</sub>] (Cambridge Isotope Laboratories). Cells were lysed and proteins were precipitated, redissolved, and digested. Thereafter, peptides were purified using reversed-phase Sep-Pak C18 cartridges (Waters). Phosphorylated peptides were enriched and fractionated. Peptide fractions were analyzed on a quadrupole Orbitrap mass spectrometer (QExactive Plus, Thermo Scientific) equipped with a UHPLC system (EASY-nLC 1000, Thermo Scientific). Survey full-scan MS spectra were acquired in the Orbitrap. The 10 most intense ions were sequentially isolated and fragmented by higher energy C-trap dissociation (HCD). Fragment spectra were acquired in the Orbitrap mass analyzer. Raw data files were analyzed using MaxQuant (dev. version 1.5.2.8). Parent ion and MS2 spectra were searched against a database containing 95,057 human protein sequences obtained from the UniProtKB released in May 2018 using Andromeda search engine. Site localization probabilities were determined by MaxQuant using the PTM scoring algorithm as described previously [70]. The dataset was filtered based on posterior error probability to arrive at a false discovery rate below 1% estimated using a target-decoy approach [71]. Only phosphorylated peptides with a score  $\geq 40$ , delta score  $\geq 8$ , score difference  $\geq 5$ , and localization probability  $\geq 0.75$  were considered for downstream analysis. The mass spectrometry proteomics data have been deposited to the ProteomeXchange Consortium via the PRIDE [72] partner repository with the dataset identifier PXD013719.

## Statistics

Statistical significance was determined by One-Way ANOVA or *t*-test in dependence of the normal distribution or variance differences of the samples using SIGMA STAT (SPSS Science). Statistical significance was accepted at a level of  $P \leq 0.05$ . The results are expressed as mean  $\pm$  standard deviation (SD) or standard error of the mean (SEM).

## Acknowledgments

We kindly thank Drs Yushan Zhu and Quan Chen (Nankai, China) for supplying the ATG9A phospho-specific antibody and Sandra Ritz (IMB, Mainz,

Germany) for her support with the live cell imaging. We also thank Marion Basoglu from the Electron Microscopy Facility of the Biology department, Frankfurt, for her help with the TEM sample preparation and imaging. This work is supported by the Collaborative Research Center CRC1177 of the DFG (to AK, CB, PB and SE), the Heller Foundation (to CB), and the Emmy Noether Program BE 5342/1-1 of the DFG (to PB).

## Credit Author Statement

FB, DS, AF, and HH carried out the experiments. SE conducted the electron microscopy. TJ and PB performed the phosphoproteomics analysis. FB, DS, TJ, PB, CB, and AK analyzed the data. CB and AK designed the study and wrote the manuscript with contributions from FB and DS.

## Conflicts of Interest

The authors declare no conflict of interest.

## Appendix A. Supplementary data

Supplementary data to this article can be found online at <https://doi.org/10.1016/j.jmb.2019.12.031>.

Received 7 August 2019;  
Received in revised form 16 December 2019;  
Accepted 16 December 2019  
Available online 24 December 2019

**Keywords:**  
autophagy;  
lipid droplets;  
autophagosome formation;  
ATG9A phosphorylation;  
adaptation

<sup>†</sup>F.B. and D.S. contributed equally to this work.

### Abbreviations used:

ATG, autophagy related; ER, endoplasmic reticulum; KO, knockout; LC3, microtubule-associated protein 1 light chain 3 beta; LD, lipid droplet; TAG, triacylglyceride; WARBM, Warburg micro syndrome; WT, wild type.

## References

- [1] T. Kawabata, T. Yoshimori, Beyond starvation: an update on the autophagic machinery and its functions, *J. Mol. Cell. Cardiol.* 95 (2016) 2–10.
- [2] C. He, D.J. Klionsky, Regulation mechanisms and signaling pathways of autophagy, *Annu. Rev. Genet.* 43 (2009) 67–93.
- [3] T.J. Mercer, A. Gubas, S.A. Tooze, A molecular perspective of mammalian autophagosome biogenesis, *J. Biol. Chem.* 293 (2018) 5386–5395.
- [4] E.L. Axe, S.A. Walker, M. Manifava, P. Chandra, H.L. Roderick, A. Habermann, et al., Autophagosome formation from membrane compartments enriched in phosphatidylinositol 3-phosphate and dynamically connected to the endoplasmic reticulum, *J. Cell Biol.* 182 (2008) 685–701.
- [5] M. Hayashi-Nishino, N. Fujita, T. Noda, A. Yamaguchi, T. Yoshimori, A. Yamamoto, A subdomain of the endoplasmic reticulum forms a cradle for autophagosome formation, *Nat. Cell Biol.* 11 (2009) 1433–1437.
- [6] E. Karanasios, E. Stapleton, M. Manifava, T. Kaizuka, N. Mizushima, S.A. Walker, et al., Dynamic association of the ULK1 complex with omegasomes during autophagy induction, *J. Cell Sci.* 126 (2013) 5224–5238.
- [7] D.J. Klionsky, B.A. Schulman, Dynamic regulation of macroautophagy by distinctive ubiquitin-like proteins, *Nat. Struct. Mol. Biol.* 21 (2014) 336–345.
- [8] H.C. Dooley, M. Razi, H.E. Polson, S.E. Girardin, M.I. Wilson, S.A. Tooze, WIP12 links LC3 conjugation with PI3P, autophagosome formation, and pathogen clearance by recruiting Atg12-5-16L1, *Mol. Cell* 55 (2014) 238–252.
- [9] N. Fujita, T. Itoh, H. Omori, M. Fukuda, T. Noda, T. Yoshimori, The Atg16L complex specifies the site of LC3 lipidation for membrane biogenesis in autophagy, *Mol. Biol. Cell* 19 (2008) 2092–2100.
- [10] J. Geng, D.J. Klionsky, The Atg8 and Atg12 ubiquitin-like conjugation systems in macroautophagy. 'Protein modifications: beyond the usual suspects' review series, *EMBO Rep.* 9 (2008) 859–864.
- [11] T. Hanada, N.N. Noda, Y. Satomi, Y. Ichimura, Y. Fujioka, T. Takao, et al., The Atg12-Atg5 conjugate has a novel E3-like activity for protein lipidation in autophagy, *J. Biol. Chem.* 282 (2007) 37298–37302.
- [12] A.H. Lystad, S.R. Carlsson, L.R. de la Ballina, K.J. Kauffman, S. Nag, T. Yoshimori, et al., Distinct functions of ATG16L1 isoforms in membrane binding and LC3B lipidation in autophagy-related processes, *Nat. Cell Biol.* 21 (2019) 372–383.
- [13] H. Weidberg, E. Shvets, T. Shpilka, F. Shimron, V. Shinder, Z. Elazar, LC3 and GATE-16/GABARAP subfamilies are both essential yet act differently in autophagosome biogenesis, *EMBO J.* 29 (2010) 1792–1802.
- [14] D.C. Rubinsztein, T. Shpilka, Z. Elazar, Mechanisms of autophagosome biogenesis, *Curr. Biol.* 22 (2012) R29–R34.
- [15] N. Dupont, S. Chauhan, J. Arko-Mensah, E.F. Castillo, A. Masedunskas, R. Weigert, et al., Neutral lipid stores and lipase PNPLA5 contribute to autophagosome biogenesis, *Curr. Biol.* 24 (2014) 609–620.
- [16] F. Moretti, P. Bergman, S. Dodgson, D. Marcellin, I. Claerr, J.M. Goodwin, et al., TMEM41B is a novel regulator of autophagy and lipid mobilization, *EMBO Rep.* (2018), <https://doi.org/10.15252/embr.201845889>.
- [17] T. Shpilka, E. Welter, N. Borovsky, N. Amar, M. Mari, F. Reggiori, et al., Lipid droplets and their component triglycerides and sterol esters regulate autophagosome biogenesis, *EMBO J.* 34 (2015) 2117–2131.
- [18] A.P. Velazquez, T. Tatsuta, R. Ghillebert, I. Drescher, M. Graef, Lipid droplet-mediated ER homeostasis regulates

- autophagy and cell survival during starvation, *J. Cell Biol.* 212 (2016) 621–631.
- [19] M. Mari, J. Griffith, E. Rieter, L. Krishnappa, D.J. Klionsky, F. Reggiori, An Atg9-containing compartment that functions in the early steps of autophagosome biogenesis, *J. Cell Biol.* 190 (2010) 1005–1022.
- [20] A. Orsi, M. Razi, H.C. Dooley, D. Robinson, A.E. Weston, L.M. Collinson, et al., Dynamic and transient interactions of Atg9 with autophagosomes, but not membrane integration, are required for autophagy, *Mol. Biol. Cell* 23 (2012) 1860–1873.
- [21] A.R. Young, E.Y. Chan, X.W. Hu, R. Kochl, S.G. Crawshaw, S. High, et al., Starvation and ULK1-dependent cycling of mammalian Atg9 between the TGN and endosomes, *J. Cell Sci.* 119 (2006) 3888–3900.
- [22] K. Imai, F. Hao, N. Fujita, Y. Tsuji, Y. Oe, Y. Araki, et al., Atg9A trafficking through the recycling endosomes is required for autophagosome formation, *J. Cell Sci.* 129 (2016) 3781–3791.
- [23] K. Soreng, M.J. Munson, C.A. Lamb, G.T. Bjorndal, S. Pankiv, S.R. Carlsson, et al., SNX18 regulates ATG9A trafficking from recycling endosomes by recruiting Dynamin-2, *EMBO Rep.* 19 (2018).
- [24] E. Zavodszky, M. Vicinanza, D.C. Rubinsztein, Biology and trafficking of ATG9 and ATG16L1, two proteins that regulate autophagosome formation, *FEBS Lett.* 587 (2013) 1988–1996.
- [25] D. Judith, H.B.J. Jefferies, S. Boeing, D. Frith, A.P. Snijders, S.A. Tooze, ATG9A shapes the forming autophagosome through Arfaptin 2 and phosphatidylinositol 4-kinase IIIbeta, *J. Cell Biol.* 218 (2019) 1634–1652.
- [26] D. Papinski, M. Schuschnig, W. Reiter, L. Wilhelm, C.A. Barnes, A. Maiolica, et al., Early steps in autophagy depend on direct phosphorylation of Atg9 by the Atg1 kinase, *Mol. Cell* 53 (2014) 471–483.
- [27] C. Zhou, K. Ma, R. Gao, C. Mu, L. Chen, Q. Liu, et al., Regulation of mATG9 trafficking by Src- and ULK1-mediated phosphorylation in basal and starvation-induced autophagy, *Cell Res.* 27 (2017) 184–201.
- [28] A. Pol, S.P. Gross, R.G. Parton, Review: biogenesis of the multifunctional lipid droplet: lipids, proteins, and sites, *J. Cell Biol.* 204 (2014) 635–646.
- [29] H.F. Hashemi, J.M. Goodman, The life cycle of lipid droplets, *Curr. Opin. Cell Biol.* 33 (2015) 119–124.
- [30] A. Sathyanarayan, M.T. Mashek, D.G. Mashek, ATGL promotes autophagy/lipophagy via SIRT1 to control hepatic lipid droplet catabolism, *Cell Rep.* 19 (2017) 1–9.
- [31] S. Martin, K. Driessens, S.J. Nixon, M. Zerial, R.G. Parton, Regulated localization of Rab18 to lipid droplets: effects of lipolytic stimulation and inhibition of lipid droplet catabolism, *J. Biol. Chem.* 280 (2005) 42325–42335.
- [32] A. Feldmann, F. Bekbulat, H. Huesmann, S. Ulbrich, J. Tatzelt, C. Behl, et al., The RAB GTPase RAB18 modulates macroautophagy and proteostasis, *Biochem. Biophys. Res. Commun.* 486 (2017) 738–743.
- [33] S. Ozeki, J. Cheng, K. Tauchi-Sato, N. Hatano, H. Taniguchi, T. Fujimoto, Rab18 localizes to lipid droplets and induces their close apposition to the endoplasmic reticulum-derived membrane, *J. Cell Sci.* 118 (2005) 2601–2611.
- [34] M.R. Pulido, A. Diaz-Ruiz, Y. Jimenez-Gomez, S. Garcia-Navarro, F. Gracia-Navarro, F. Tinahones, et al., Rab18 dynamics in adipocytes in relation to lipogenesis, lipolysis and obesity, *PLoS One* 6 (2011), e22931.
- [35] D. Xu, Y. Li, L. Wu, Y. Li, D. Zhao, J. Yu, et al., Rab18 promotes lipid droplet (LD) growth by tethering the ER to LDs through SNARE and NRZ interactions, *J. Cell Biol.* 217 (2018) 975–995.
- [36] C. Li, X. Luo, S. Zhao, G.K. Siu, Y. Liang, H.C. Chan, et al., COPI-TRAPPII activates Rab18 and regulates its lipid droplet association, *EMBO J.* 36 (2017) 441–457.
- [37] D. Li, Y.G. Zhao, D. Li, H. Zhao, J. Huang, G. Miao, et al., The ER-localized protein DFCP1 modulates ER-lipid droplet contact formation, *Cell Rep.* 27 (2019) 343–358 e5.
- [38] C.B.K. Jayson, H. Arlt, A.W. Fischer, Z.W. Lai, R.V. Farese Jr., T.C. Walther, Rab18 is not necessary for lipid droplet biogenesis or turnover in human mammary carcinoma cells, *Mol. Biol. Cell* 29 (2018) 2045–2054.
- [39] S.M. Carpanini, L. McKie, D. Thomson, A.K. Wright, S.L. Gordon, S.L. Roche, et al., A novel mouse model of Warburg Micro syndrome reveals roles for RAB18 in eye development and organisation of the neuronal cytoskeleton, *Dis. Model Mech.* 7 (2014) 711–722.
- [40] R.P. Liegel, M.T. Handley, A. Ronchetti, S. Brown, L. Langemeyer, A. Linford, et al., Loss-of-function mutations in TBC1D20 cause cataracts and male infertility in blind sterile mice and Warburg micro syndrome in humans, *Am. J. Hum. Genet.* 93 (2013) 1001–1014.
- [41] A. Gerondopoulos, R.N. Bastos, S. Yoshimura, R. Anderson, S. Carpanini, I. Aligianis, et al., Rab18 and a Rab18 GEF complex are required for normal ER structure, *J. Cell Biol.* 205 (2014) 707–720.
- [42] M.T. Handley, I.A. Aligianis, RAB3GAP1, RAB3GAP2 and RAB18: disease genes in Micro and Martolf syndromes, *Biochem. Soc. Trans.* 40 (2012) 1394–1397.
- [43] A.S. Rambold, S. Cohen, J. Lippincott-Schwartz, Fatty acid trafficking in starved cells: regulation by lipid droplet lipolysis, autophagy, and mitochondrial fusion dynamics, *Dev. Cell* 32 (2015) 678–692.
- [44] M. Schweiger, G. Schoiswohl, A. Lass, F.P. Radner, G. Haemmerle, R. Malli, et al., The C-terminal region of human adipose triglyceride lipase affects enzyme activity and lipid droplet binding, *J. Biol. Chem.* 283 (2008) 17211–17220.
- [45] R. Zimmermann, J.G. Strauss, G. Haemmerle, G. Schoiswohl, R. Birner-Gruenberger, M. Riederer, et al., Fat mobilization in adipose tissue is promoted by adipose triglyceride lipase, *Science* 306 (2004) 1383–1386.
- [46] T.C. Walther, J. Chung, R.V. Farese Jr., Lipid droplet biogenesis, *Annu. Rev. Cell Dev. Biol.* 33 (2017) 491–510.
- [47] V.T. Salo, I. Belevich, S. Li, L. Karhinen, H. Vihtinen, C. Vigouroux, et al., Seipin regulates ER-lipid droplet contacts and cargo delivery, *EMBO J.* 35 (2016) 2699–2716.
- [48] M. Rosner, N. Siegel, A. Valli, C. Fuchs, M. Hengstschlager, mTOR phosphorylated at S2448 binds to raptor and rictor, *Amino Acids* 38 (2010) 223–228.
- [49] D.F. Egan, D.B. Shackelford, M.M. Mihaylova, S. Gelino, R.A. Kohnz, W. Mair, et al., Phosphorylation of ULK1 (hATG1) by AMP-activated protein kinase connects energy sensing to mitophagy, *Science* 331 (2011) 456–461.
- [50] J. Kim, M. Kundu, B. Viollet, K.L. Guan, AMPK and mTOR regulate autophagy through direct phosphorylation of Ulk1, *Nat. Cell Biol.* 13 (2011) 132–141.
- [51] T. Osawa, T. Kotani, T. Kawaoka, E. Hirata, K. Suzuki, H. Nakatogawa, et al., Atg2 mediates direct lipid transfer between membranes for autophagosome formation, *Nat. Struct. Mol. Biol.* 26 (2019) 281–288.

- [52] D.P. Valverde, S. Yu, V. Boggavarapu, N. Kumar, J.A. Lees, T. Walz, et al., ATG2 transports lipids to promote autophagosome biogenesis, *J. Cell Biol.* (2019), <https://doi.org/10.1083/jcb.201811139>.
- [53] S.Y. Dejgaard, A. Murshid, A. Erman, O. Kizilay, D. Verbich, R. Lodge, et al., Rab18 and Rab43 have key roles in ER-Golgi trafficking, *J. Cell Sci.* 121 (2008) 2768–2781.
- [54] S.Y. Dejgaard, J.F. Presley, Rab18: new insights into the function of an essential protein, *Cell. Mol. Life Sci.* 76 (2019) 1935–1945.
- [55] E. Smirnova, E.B. Goldberg, K.S. Makarova, L. Lin, W.J. Brown, C.L. Jackson, ATGL has a key role in lipid droplet/adiposome degradation in mammalian cells, *EMBO Rep.* 7 (2006) 106–113.
- [56] A. Lass, R. Zimmermann, G. Haemmerle, M. Riederer, G. Schoiswohl, M. Schweiger, et al., Adipose triglyceride lipase-mediated lipolysis of cellular fat stores is activated by CGI-58 and defective in Chanarin-Dorfman Syndrome, *Cell Metabol.* 3 (2006) 309–319.
- [57] X. Yang, X. Lu, M. Lombes, G.B. Rha, Y.I. Chi, T.M. Guerin, et al., The G(0)/G(1) switch gene 2 regulates adipose lipolysis through association with adipose triglyceride lipase, *Cell Metabol.* 11 (2010) 194–205.
- [58] A. Kern, I. Dikic, C. Behl, The integration of autophagy and cellular trafficking pathways via RAB GAPs, *Autophagy* 11 (2015) 2393–2397.
- [59] N. Spang, A. Feldmann, H. Huesmann, F. Bekbulat, V. Schmitt, C. Hiebel, et al., RAB3GAP1 and RAB3GAP2 modulate basal and rapamycin-induced autophagy, *Autophagy* 10 (2014) 2297–2309.
- [60] N. Mizushima, H. Sugita, T. Yoshimori, Y. Ohsumi, A new protein conjugation system in human. The counterpart of the yeast Apg12p conjugation system essential for autophagy, *J. Biol. Chem.* 273 (1998) 33889–33892.
- [61] C. Kishi-Itakura, I. Koyama-Honda, E. Itakura, N. Mizushima, Ultrastructural analysis of autophagosome organization using mammalian autophagy-deficient cells, *J. Cell Sci.* 127 (2014) 4089–4102.
- [62] K. Tsuboyama, I. Koyama-Honda, Y. Sakamaki, M. Koike, H. Morishita, N. Mizushima, The ATG conjugation systems are important for degradation of the inner autophagosomal membrane, *Science* 354 (2016) 1036–1041.
- [63] J.O. Pyo, S.M. Yoo, H.H. Ahn, J. Nah, S.H. Hong, T.I. Kam, et al., Overexpression of Atg5 in mice activates autophagy and extends lifespan, *Nat. Commun.* 4 (2013) 2300.
- [64] A.K. Velikkakath, T. Nishimura, E. Oita, N. Ishihara, N. Mizushima, Mammalian Atg2 proteins are essential for autophagosome formation and important for regulation of size and distribution of lipid droplets, *Mol. Biol. Cell* 23 (2012) 896–909.
- [65] D. Bakula, A.J. Muller, T. Zuleger, Z. Takacs, M. Franz-Wachtel, A.K. Thost, et al., WIPI3 and WIPI4 beta-propellers are scaffolds for LKB1-AMPK-TSC signalling circuits in the control of autophagy, *Nat. Commun.* 8 (2017) 15637.
- [66] N. Tamura, T. Nishimura, Y. Sakamaki, I. Koyama-Honda, H. Yamamoto, N. Mizushima, Differential requirement for ATG2A domains for localization to autophagic membranes and lipid droplets, *FEBS Lett.* 591 (2017) 3819–3830.
- [67] J.F. Gilles, M. Dos Santos, T. Boudier, S. Bolte, N. Heck, DiAna, An ImageJ tool for object-based 3D co-localization and distance analysis, *Methods* 115 (2017) 55–64.
- [68] D.J. Klionsky, K. Abdelmohsen, A. Abe, M.J. Abedin, H. Abeliovich, A. Acevedo Arozena, et al., Guidelines for the use and interpretation of assays for monitoring autophagy (3rd edition), *Autophagy* 12 (2016) 1–222.
- [69] M.E. Borisova, S.A. Wagner, P. Beli, Mass spectrometry-based proteomics for quantifying DNA damage-induced phosphorylation, *Methods Mol. Biol.* 1599 (2017) 215–227.
- [70] J. Cox, M. Mann, MaxQuant enables high peptide identification rates, individualized p.p.b.-range mass accuracies and proteome-wide protein quantification, *Nat. Biotechnol.* 26 (2008) 1367–1372.
- [71] J.E. Elias, S.P. Gygi, Target-decoy search strategy for increased confidence in large-scale protein identifications by mass spectrometry, *Nat. Methods* 4 (2007) 207–214.
- [72] Y. Perez-Riverol, A. Csordas, J. Bai, M. Bernal-Llinares, S. Hewapathirana, D.J. Kundu, et al., The PRIDE database and related tools and resources in 2019: improving support for quantification data, *Nucleic Acids Res.* 47 (2019) D442–D450.